Materials Science-Poland, 40(4), 2022, pp. 91-103
http://www.materialsscience.pwr.wroc.pl/
DOI: 10.2478/msp-2022-0026

sciendo

The structure and properties of laser-cladded Inconel 625/TiC composite coatings

Aleksandra Lont[1,*], Tomasz Poloczek[1], Jacek Górka[1]

[1]Welding Department, Faculty of Mechanical Engineering, Silesian University of Technology, Konarskiego Street 18A, 44-100 Gliwice, Poland

The article presents the research in the field of production of metal–matrix composite coatings using laser cladding technology. The general purpose of producing composite coatings is the improvement of wear resistance of the material surface. In this research, Inconel 625 was used as a matrix material. Nickel-based superalloys are used in several industries for unique applications because they possess a number of beneficial properties including high tensile and fatigue strengths and resistance to high-temperature corrosion in aggressive environments. However, for some applications, this alloy shows insufficient wear resistance of the surface; therefore, for the tests, Inconel 625-based composite coatings were produced with the addition of 10 vol.%, 20 vol.%, and 40 vol.% of titanium carbide (TiC) particles as reinforcement. In general, the addition of TiC particles had a positive effect on the erosion resistance of the surface. The aim of the current research was to test the influence of TiC particle reinforcement of Inconel 625 laser-cladded coatings on corrosion resistance of the surface. For the tests, the laser-cladded composite coatings with uniform phase distribution were produced. The proceeded tests included penetrant tests, macrostructure and microstructure analysis, X-ray diffraction (XRD), and microhardness and corrosion resistance tests. The results showed that using laser cladding, TiC-reinforced Inconel 625 uniform composite coatings may be produced. The addition of TiC particles caused microstructure changes in the Inconel 625 matrix and an increase in hardness. The addition of TiC particles had a negative influence on Inconel 625 corrosion resistance, but with the increased composite coating homogeneity, the corrosion resistance improved.

Keywords: *composite coatings, nickel-based superalloys, laser cladding*

RETRACTED

1. Introduction

Surface engineering technologies are widely used for the enhancement of surface properties such as corrosion or wear resistance [1] while maintaining the favorable properties of the processed material core (e.g., mechanical and plastic properties) [2]. Nickel-based superalloys are widely used as coating materials due to their high corrosion resistance under aggressive environments and high temperatures [3], high tensile and fatigue strength, high-temperature toughness, and ductility [4]. The positive influence of Inconel 625 coatings on the corrosion resistance of various grades of low-alloy and stainless steel has been reported [5].

For the purposes of wear resistance improvement of the surface, the metal matrix composite (MMC) coatings [6] or surface layers [7] reinforced with ceramic particles are commonly used. The production of composite coatings with the nickel-based superalloy matrix has a high application potential due to numerous beneficial properties of these alloys combined with increased wear resistance [8]. The previously conducted studies in this field proved that the production of nickel-based superalloy coatings reinforced with carbides (WC [9], Cr_2C_3 [10], VC [11], TiC [12]), BN [13, 14], TiB_2 [15], carbon nanotubes [16], and graphene nanoplatelets [17] provides the enhancement of the mechanical properties and wear resistance in comparison to metallic coatings. In the case of the production of MMC coatings based on the nickel-based superalloys characterized by high-temperature corrosion resistance, it is reasonable to select a reinforcement material with high thermal stability [18]. The ceramic material commonly used as composite reinforcement, which

* E-mail: Aleksandra.Lont@polsl.pl

© Aleksandra Lont et al. 2022. This is an open access article distributed under the Creative Commons Attribution-NonCommercial-NoDerivatives 4.0 License. (http://creativecommons.org/licenses/by-nc-nd/4.0/)

is characterized by high melting point (3,180°C) and thermal stability, high hardness (2,859–3,200 HV), strength (240–390 MPa), and low density (4.93 g/cm^3), is titanium carbide (TiC) [19]. The previous research showed that the homogeneous nickel-based superalloy composite coatings reinforced with TiC particles in various contents can be produced using laser cladding technology [20]. Cao and Gu's research results [21] revealed that the Inconel 625-based laser-cladded coatings reinforced with 2.5% nano-TiC show higher hardness and lower coefficient of friction and wear rate than pure Inconel 625. Jiang et al. [22] produced Inconel 625-based composite coatings reinforced with 5% nano-TiC particles, which resulted in an increase in hardness and modulus in comparison to metallic Inconel 625 coatings. Lian et al. [23] produced Ni35A-based laser-cladded coatings reinforced with 20%–80% of TiC particles. The research results showed that the increase in the TiC powder ratio resulted in an increase in hardness and wear resistance. Based on the research results, it is clear that the Inconel 625-based composite coatings reinforced with TiC particles show higher wear resistance and hardness than pure Inconel 625 coatings. The addition of TiC particles to Inconel 625 coatings results in the microstructure changes, which may influence the corrosion resistance. In the case of the production of coatings, working in conditions of both surface wear and aggressive corrosive environment, it is very important to produce wear-resistant coatings in which the addition of reinforcement will not deteriorate the corrosion resistance. Ge et al. [24] conducted research on the corrosion resistance of Inconel 625-based coatings reinforced with 4% TiC particles depending on the laser cladding process parameters. Bakkar et al. [25] tested the corrosion resistance of Inconel 625/TiC composites produced by the squeeze casting technique. The results showed that the addition of 25% of TiC did not affect the corrosion resistance of Inconel 625, while higher fractions influenced the deterioration of corrosion resistance.

The aim of this research was the production of Inconel 625-based composite coatings reinforced with 10%, 20%, and 40% of TiC particles using laser cladding. The tests conducted include penetrant tests, macrostructure and microstructure observations, chemical and phase composition analyses, microhardness tests, and potentiodynamic polarization corrosion tests.

2. Materials and Methodology

The laser cladding of metallic Inconel 625 and composite Inconel625/TiC coatings was conducted on the 10-mm-thick, as-received low-alloy steel S355JR substrate with dimensions of 100 mm × 100 mm. The substrate surface was prepared by grinding and degreasing using ethyl alcohol. For the laser cladding process, the Inconel 625 (Oerlikon Metcoclad 625 gas atomized powder) and 99.8% pure TiC (Goodfellow TI546030/2) powders were mixed in Inconel 625-to-TiC volume ratios of 100:0, 90:10, 80:20, and 60:40. The powders were dried for 1 h at 50°C before the laser cladding process. The chemical compositions of the substrate material and Inconel 625 powder are presented in Table 1.

For the laser cladding process, the stand equipped with a disc laser TRUMPF Trudisc 3302—the numerically controlled system for positioning the processed material in relation to the laser head and gravitational powder feeding system—was used. The laser beam focus (diameter of 200 μm) was set 30 mm above the substrate surface. The powder was injected directly into the molten pool. Argon was used as shielding and powder transporting gas with flow rates of 10 l/min and 3 l/min, respectively. For the tests, the multi-run coatings were produced with a 40% overlap. The laser cladding process was carried out without preheating and the interpass temperature was max. 30°C. The process parameters (Table 2) were chosen based on the previous experience [26].

The penetrant tests were conducted using the color contrast technique using penetrant MR 68 NF, developer MR 70, and cleaner MR 79. The macrostructure analysis included macrostructure observations on a scanning electron microscope (SEM) Phenom World Pro with the quality and homogeneity assessment, the coating dilution calculations using Eq. (1); the measurements of the cross-sectional area using Autodesk AutoCAD 2018 soft-

RETRACTED

Table 1. Chemical composition of S355JR substrate and Metcoclad 625 powder

Material designation	**C**	**Mn**	**Si**	**P**	**S**	**Cr**	**Ni**	**Mo**	**Nb**	**Al**	**Cu**	**Fe**
	wt.%											
S355JR	0.2	1.5	0.2–0.5	Max. 0.04	Max. 0.04	Max. 0.3	Max. 0.3	-	-	Max. 0.02	Max. 0.03	Balance
Oerlikon Metcoclad 625	-	-	-	-	-	20.0–23.0	58.0–63.0	8.0–10.0	3.0–5.0	-	-	Max 5.0

Table 2. Laser cladding parameters

Designation	**Powder TiC content (vol.%)**	**Laser power (W)**	**Speed (m/min)**	**Powder feed rate (g/mm)**
M1	0	2.100	0.25	0.04
M2				0.05
C1	10			0.04
C2				0.05
C3	20			0.04
C4				0.05
C5	40			0.04
C6				0.05

ware, and the TiC fraction measurements using Image-Pro Plus software.

$$U = \frac{F_{BM}}{F_{BM} + RA} \times 100\% \quad (1)$$

where F_{BM} is the cross-sectional area of the melted substrate and RA is the cross-sectional area of reinforcement of the clad.

The microstructure observations and energy-dispersive spectroscopy (EDS) chemical composition analysis were proceeded using SEM Phenom World Pro. The specimens for macrostructure and microstructure observations were cut at a distance of 50 mm from the beginning of laser processing, where the process was stable. For etching, the mixture of HNO_3, HCl, acetic acid, and glycerol was used (etchant 89 according to ASTM E 407-99), and the specimens were heated by immersion in distilled water at a temperature of 100°C for 2 min and then etched by immersion for 10 s. The general chemical composition of coatings was estimated based on the four cross-sectional surface EDS results at a magnification of 1000x and an accelerating voltage of 15 kV. X-ray diffraction (XRD) analysis was conducted using a Malvern PANalytical X'Pert PRO diffraction system with filtered radiation from the lamp with a cobalt anode on the grounded coating surfaces. The diffraction profiles were obtained in the 2Θ range of 25°–130° in a continuous scan mode with a step size of 0.1444° and a counting time per step of 22.695 s.

The Vickers microhardness of laser-cladded coatings was measured using a Wilson 401MVD microindentation tester with a 200 g load and a dwell time of 12 s in three lines across the beads at a distance of 0.7 mm, 1.0 mm, and 1.3 mm from the surface (Figure 1A) with a distance between measuring points of 0.5 mm. Additionally, microhardness was measured in three lines from the surface to the base material, with a distance of 0.1 mm between each point of (Figure 1B).

The corrosion behavior of produced metallic and composite laser-cladded coatings was tested using potentiodynamic polarization experiments according to the ISO 17475:2010 standard. For the tests, the Autolab 302 N potentiostat equipped with a three-electrode cell controlled by NOVA software was used. The electrochemical measurements were conducted in 3.5% NaCl solution at 25°C. A saturated calomel electrode (SCE) was used as the reference electrode, and a platinum rod was used

RETRACTED

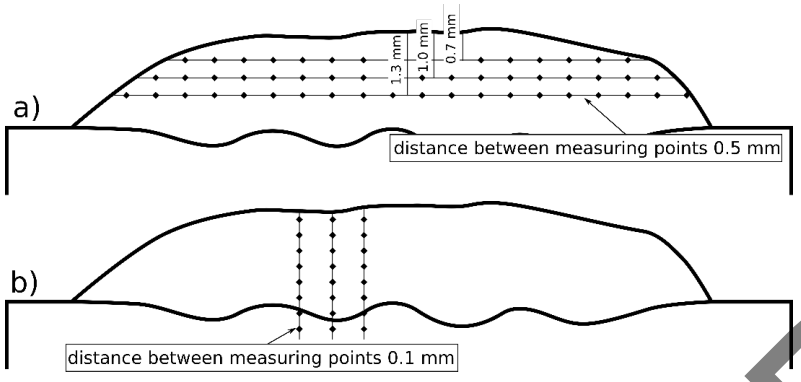

Fig. 1. Vickers microhardness measuring lines scheme: **(A)** measurements across the beads and **(B)** measurements from the surface to base material

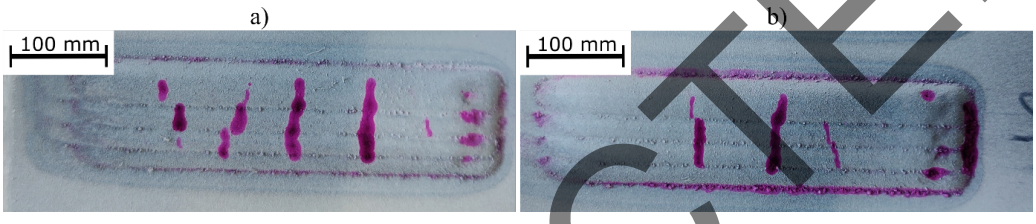

Fig. 2. Surface view of coatings after penetrant testing: **(A)** C5 and **(B)** C6 (designations according to Table 2)

as the counter electrode. The corrosion resistance was evaluated by recording the open-circuit potential (E_{OCP}) variation versus the SCE. For the tests, coating surfaces were prepared by grinding. The samples were measured after 600 s of open-circuit potential stabilization at a scan rate of 1 mVs^{-1}. The surface morphology after the electrochemical tests was analyzed using SEM Zeiss EVO MA10.

3. Results and Discussion

The penetrant tests showed linear indications caused by cracks on two coatings produced by the powder mixture with a TiC particle fraction of 40 vol.% (Figure 2). No indications were observed on the surfaces of the metallic and remaining composite coatings. The cracks on the coatings with the highest TiC particle fraction were due to higher hardness and brittleness of these coatings.

The macrographs of metallic and composite coatings are presented in Figure 3; the thicknesses, dilutions, and measured TiC fractions are summarized in Table 3; and the average chemical compositions of coatings from EDS are presented in Table 4. The test results allowed to assess the influence of the powder feed rate and TiC ratio on the thickness, penetration, dilution, and uniformity of TiC particle distribution in the structure of the coatings. The macrograph observations allowed to assess the quality of coatings. In the case of all coating laser cladded with a powder feed rate of 0.04 g/mm, no imperfections were observed on the cross-sections. The macroscopic observations also revealed that the uniformity of TiC distribution has improved with the increased TiC fraction. In the case of coatings with TiC content of 10 vol.% and 20 vol.%, the clusters of reinforcing particles were observed, mainly in the upper area of coatings, due to the lower density of TiC particles than Inconel 625. The increased powder feed rate resulted in lower penetration and dilution of the substrate, which influenced the local lack of fusion of the coatings produced with powder mixtures with a TiC content of 20 vol.% and 40 vol.%. The dilution decreased together with the increased TiC content for composite coatings produced at constant parameters, although the lowest dilution levels were measured for metallic Inconel 625 coat-

RETRACTED

Table 3. Thickness, dilution, and TiC fraction measurement results

Designation (Table 2)	Thickness (mm)	Dilution (%)	Measured TiC fraction (vol.%)
M1	1.6	3.3	-
M2	2.1	2.1	-
C1	1.7	25.5	8.8
C2	2.1	12.6	9.8
C3	1.8	17.5	18.3
C4	2.2	9.8	19.6
C5	1.9	14.6	38.6
C6	2.3	7.5	39.7

Table 4. Average chemical composition of coatings

Designation (Table 2)	Ni	Cr	Mo	Nb	Fe	Ti
	wt.%					
M1	60.7 ± 1.6	19.8 ± 0.5	10.2 ± 0.8	4.6 ± 0.1	4.7 ± 1.1	-
M2	63.6 ± 0.6	20.7 ± 0.3	9.5 ± 0.5	4.4 ± 0.6	1.8 ± 0.3	-
C1	49.1 ± 1.1	16.2 ± 0.4	8.1 ± 0.6	4.7 ± 0.4	18.0 ± 1.0	2.7 ± 0.5
C2	54.1 ± 4.7	17.6 ± 1.4	9.3 ± 1.1	4.2 ± 0.9	7.9 ± 2.6	3.5 ± 1.1
C3	50.3 ± 1.3	16.6 ± 0.2	9.7 ± 1.4	3.9 ± 0.3	14.4 ± 0.8	5.4 ± 2.1
C4	55.1 ± 1.9	18.1 ± 0.5	10.1 ± 1.3	5.1 ± 0.2	5.1 ± 1.6	6.4 ± 1.3
C5	44.1 ± 2.9	14.1 ± 2.2	7.4 ± 0.9	4.3 ± 0.5	14.5 ± 3.9	14.6 ± 3.8
C6	47.0 ± 4.9	16.0 ± 1.8	8.6 ± 1.4	4.8 ± 0.8	3.3 ± 1.9	19.7 ± 8.5

RETRACTED

ings. The higher penetration of composite coatings than metallic coatings can be attributed to the increase in laser radiation absorption, due to the presence of TiC particles in the powder. On the other hand, the TiC ratio increase led to the penetration decrease, which may result from the Marangoni convection inhibition [27]. The thickness of coatings slightly increased together with the increased powder feed rate and TiC ratio. The measured TiC fraction for each composite coatings was lower than the TiC content in the powder mixture, which is related to the dilution levels. (In each coating, the TiC fraction is higher when the dilution is lower.) The higher dilution influenced the increase in the average iron composition (Table 4).

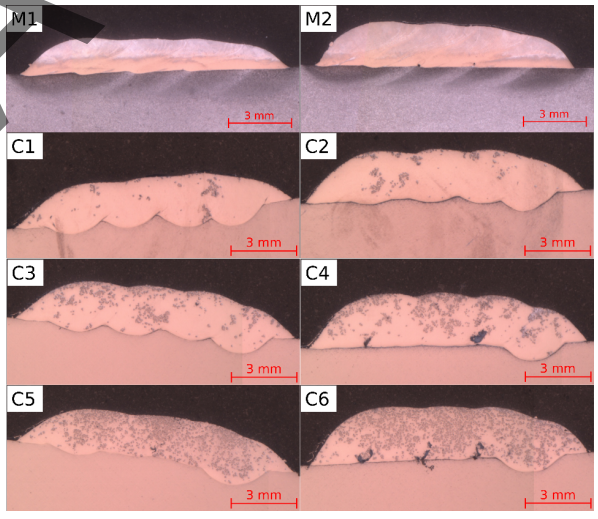

Fig. 3. Macrographs of laser-cladded coatings (designations according to Table 2)

The microstructure of TiC-reinforced composite Inconel 625 coatings is presented in Figure 4. The microstructure of metallic Inconel 625 coatings is presented in Figure 5. The matrix microstructure of composite coatings consists of austenite dendrites (confirmed by XRD results presented in Figure 6) and minor secondary phases. The EDS analysis (Figure 7) revealed that austenite dendrites are mainly composed of nickel, chromium, and iron, while the secondary phases are rich in carbon, niobium, molybdenum, and titanium. The chemical composition of used Metco-clad 625 powder does not contain titanium and carbon, so it can be assumed that the precipitation of

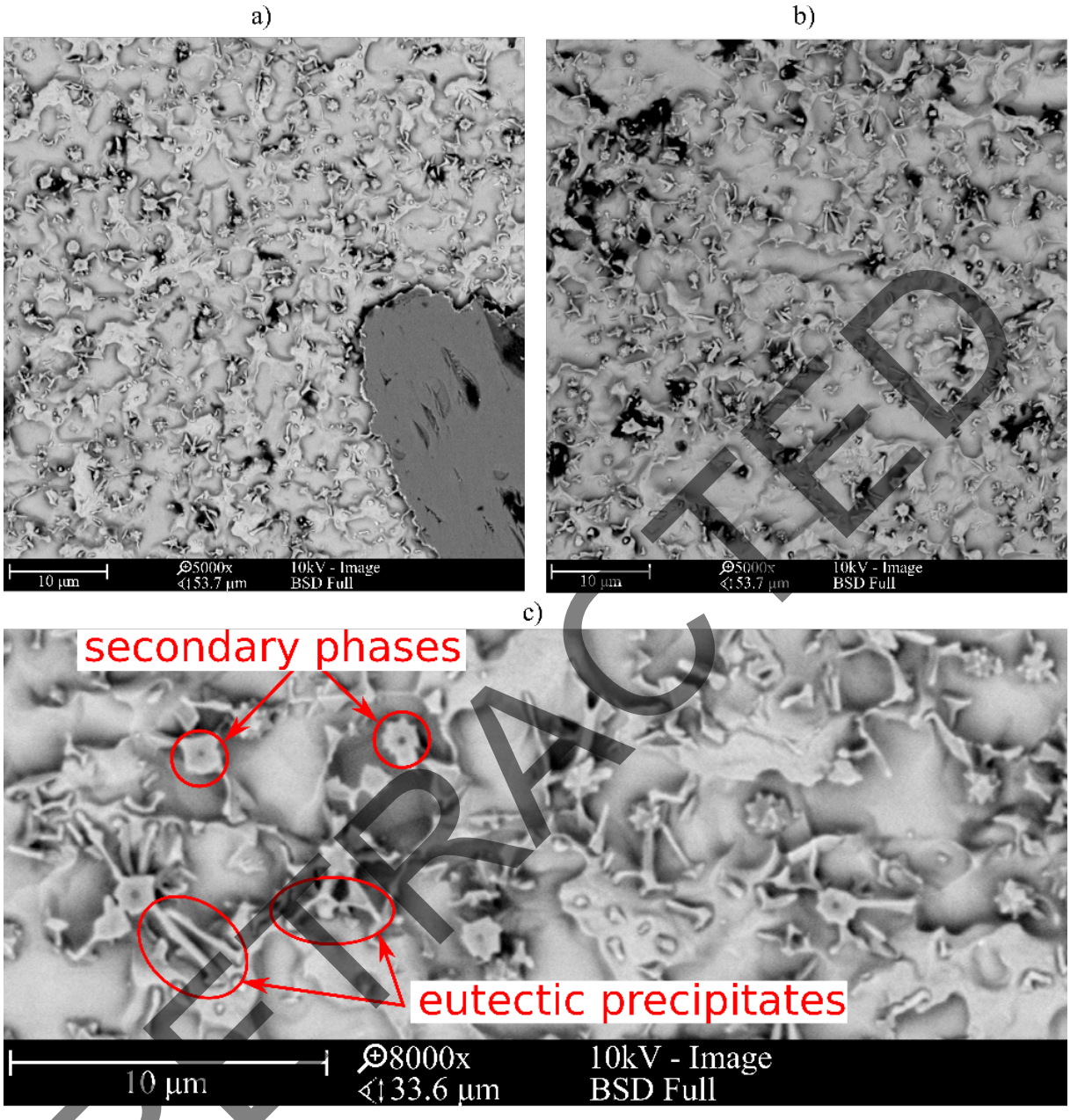

Fig. 4. Microstructure of central bead areas of composite Inconel 625/TiC coatings: **(A)** C1, **(B)** C2, and **(C)** C4 (designation according to Table 3). TiC, titanium carbide

RETRACTED

the secondary phases in the matrix occurred as a result of the partial dissolution of TiC particles in the matrix and its enrichment with carbon and titanium. This is confirmed by the metallic Inconel 625 coating microstructure observations, in which no such precipitates were observed. The metallic coatings showed a typical dendritic structure with minor constituents in the interdendritic regions, which were previously reported by Cieslak et al. [28]. The columnar growth of dendrites was observed in the case of metallic Inconel 625 coatings, which is caused by the temperature gradient, and it occurred in the direction opposite to the heat transfer direction.

The secondary phases formed in the matrix are characterized by blocky and dendritic morphology

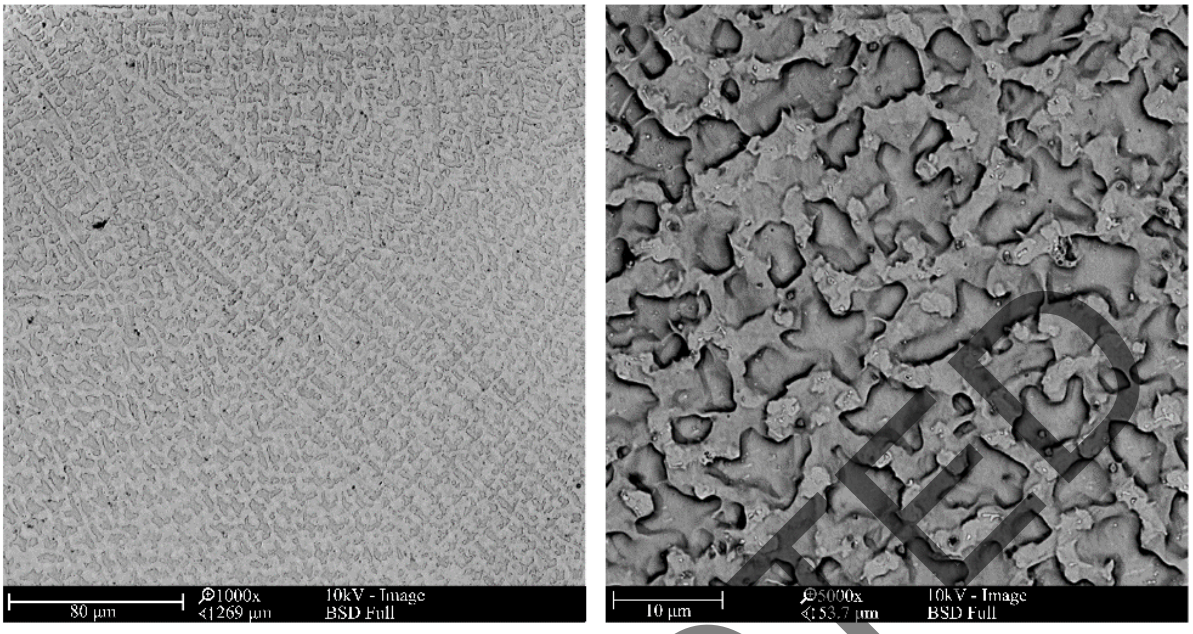

Fig. 5. Microstructure of metallic Inconel 625 coatings

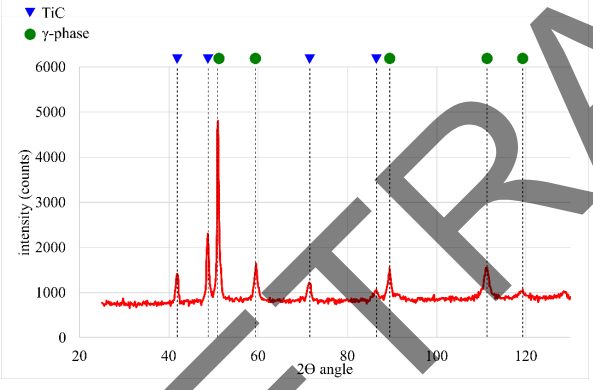

Fig. 6. XRD results of the respective composite Inconel 625/TiC coating. TiC, titanium carbide; XRD, X-ray diffraction

and showed gradient distribution of chemical composition (Figure 4). The EDS analysis revealed that the inner, darker part of these phases contains a higher contribution of titanium. It can be assumed that the TiC particles precipitated from the liquid metal and then the Mo and Nb atoms dissolved in the crystal lattice. In the matrix microstructure also, the eutectic precipitates can be observed on the secondary phases. After precipitation of secondary phases, during cooling, they acted as the crystal nucleus for eutectic precipitates between the austenite dendrites.

In the microstructure of overlap areas between consecutive beads (Figure 8), the austenite dendrites, and secondary and eutectic phase precipitates can be observed in the matrix, as in the central bead areas. Additionally, large dendritic precipitates were observed, which were formed due to the higher TiC particle dissolution resulted from the influence of the subsequent thermal cycle. In this area, the TiC particles were more rounded and showed the lighter shell around composed of carbon, niobium, molybdenum, and titanium, which is same as dendritic precipitates (Figure 9). The morphology of dendritic precipitates is a characteristic for formed in situ TiC particles [29]; therefore, it can be assumed that the TiC precipitates were formed in the overlap area, and the Nb and Mo atoms dissolved in their crystal lattice.

The Vickers microhardness results are presented in Figure 10. The average microhardness of TiC reinforced Inconel 625 coatings varies from 258 to 342 HV0.2. The addition of 10–40 vol.% of TiC particles caused the average microhardness increase by 5–50% in comparison to metallic Inconel

RETRACTED

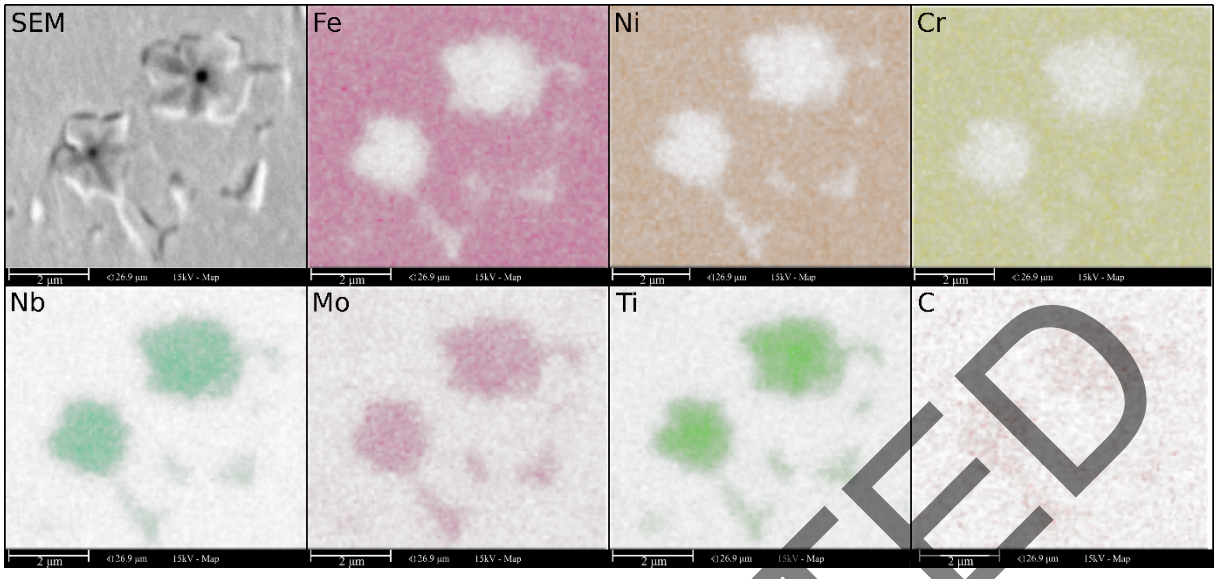

Fig. 7. EDS maps of composite Inconel 625/TiC coating matrix. EDS, energy-dispersive spectroscopy; SEM, scanning electron microscope; TiC, titanium carbide

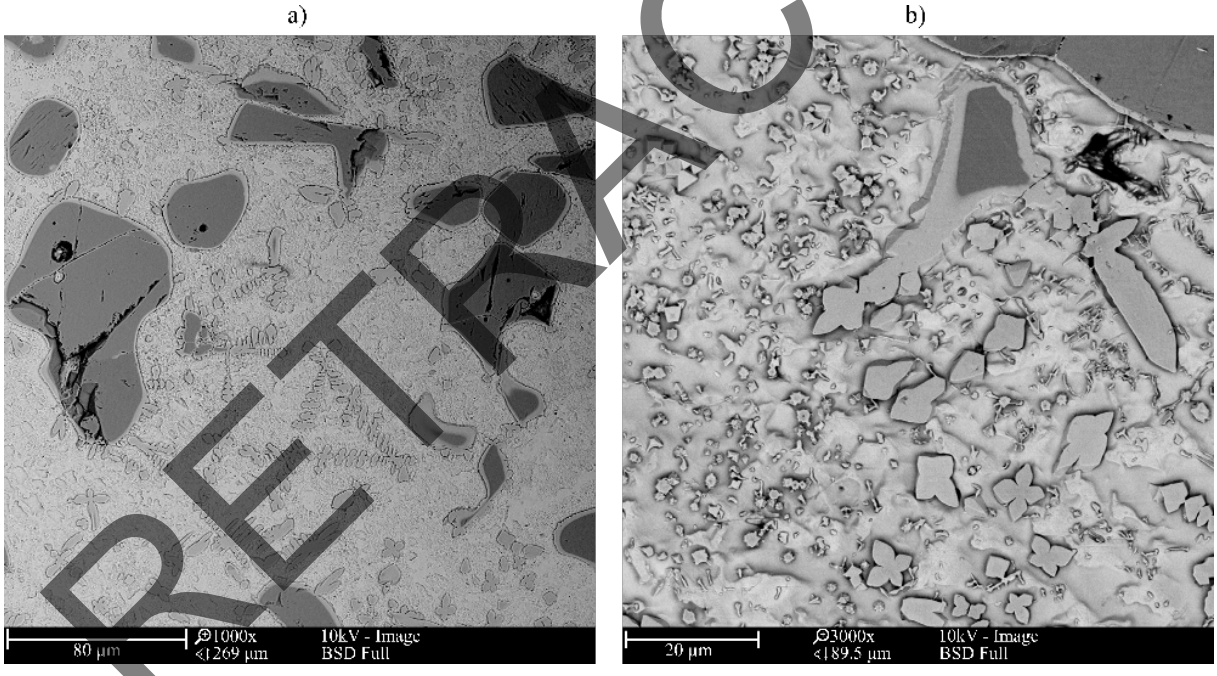

Fig. 8. Microstructure of overlap areas of composite Inconel 625/TiC coatings, magnification a) 1000x, b) 3000x TiC, titanium carbide

625 coatings. With the increase in the TiC particle content, the microhardness of coatings laser cladded with constant parameters increased. The increase in the powder feed rate during the laser cladding process using powder with the same TiC particle fraction caused the increase in the average microhardness, which is associated with the lower dilution and higher measured TiC particle content. In each of the tested coatings, no significant changes in the microhardness were reported in

RETRACTED

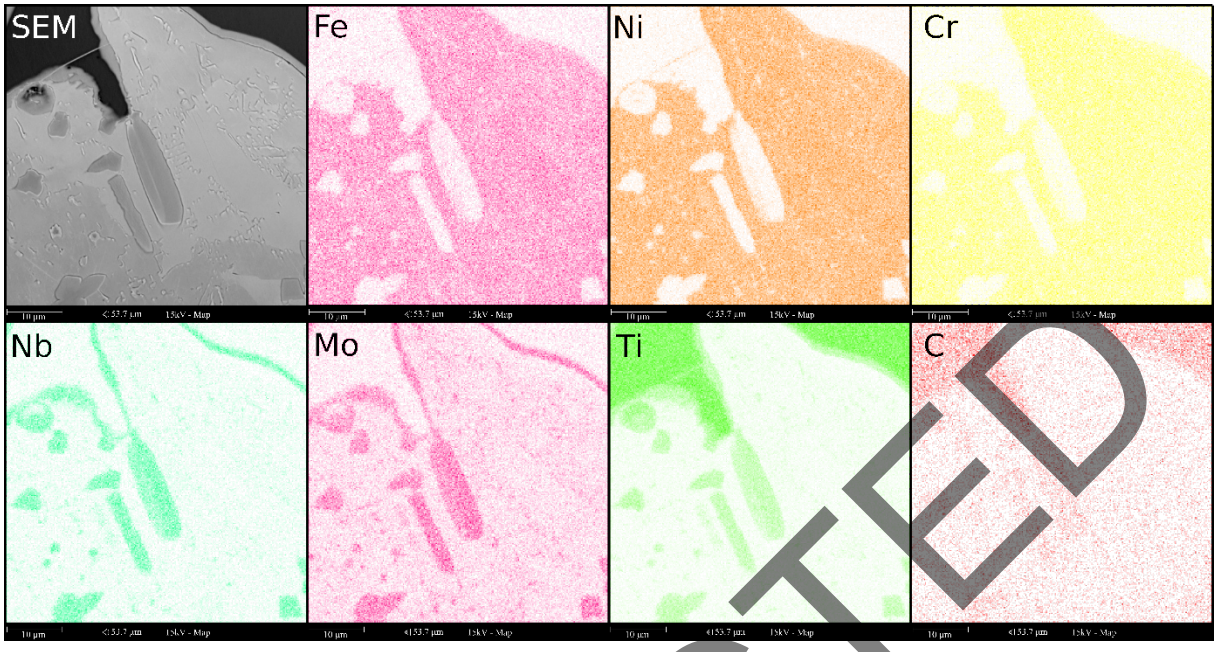

Fig. 9. EDS maps of the overlap area of composite Inconel 625/TiC coatings. EDS, energy-dispersive spectroscopy; SEM, scanning electron microscope; TiC, titanium carbide

the overlap area between consecutive beads. The slight microhardness decrease was observed toward the end of the measuring line (Figure 10B), which is caused by the higher dilution of the first bead, which can be observed in Figure 3. The microhardness distribution from the coating surface to the base material (Figure 10C) shows the highest hardness near the surface and a slight decrease toward the base material. This phenomenon is related to a higher proportion of carbides in the upper area of the coating, due to their lower density than the matrix material, and flowing upward in the molten metal pool.

The potentiodynamic polarization curves obtained for metallic Inconel 625 coatings M1 and TiC-reinforced Inconel 625 coatings C1, C3, and C5 are presented in Figure 11. The corrosion results are summarized in Table 5, and the corrosion potential (E_{corr}) and corrosion current density (j_{corr}) are acquired by using the Tafel extrapolation method. Generally, the materials that show high corrosion potential and low corrosion current density are characterized by high corrosion resistance [12]. The values of E_{corr} and j_{corr} for metallic Inconel 625 coating are −0.384 V and 8.0 μA/cm^2, respectively. For the composite coatings, the corrosion potential varied from −0.377 V to −0.473 V, while the corrosion current density was 8.9–83.0 μA/cm^2. Based on the results of the corrosion current density, the best corrosion resistance was obtained for the metallic Inconel 625 coating, while the composite coating with the TiC fraction of 38.6 vol.% (C5) revealed slightly lower corrosion resistance. The lowest corrosion resistance showed C3 composite coating (TiC fraction of 18.3 vol.%), with a 10 times higher corrosion current density than the metallic coating. Taking the results of corrosion potentials into account, out of composite coatings, the best results showed coating with the highest TiC fraction (C5), and the lowest corrosion resistance was obtained for the C3 coating. The metallic Inconel 625 coating showed a slightly lower corrosion potential than the C5 composite coating. Generally, both used materials (Inconel 625 alloy [30] and TiCs [31]) offer high corrosion resistance in the analyzed solution, but the microstructure of composite coatings may affect their corrosion resistance, for example, the uniformity, grain size, particle–matrix interface quality, and presence of the intermetallic phases [24]. Out

RETRACTED

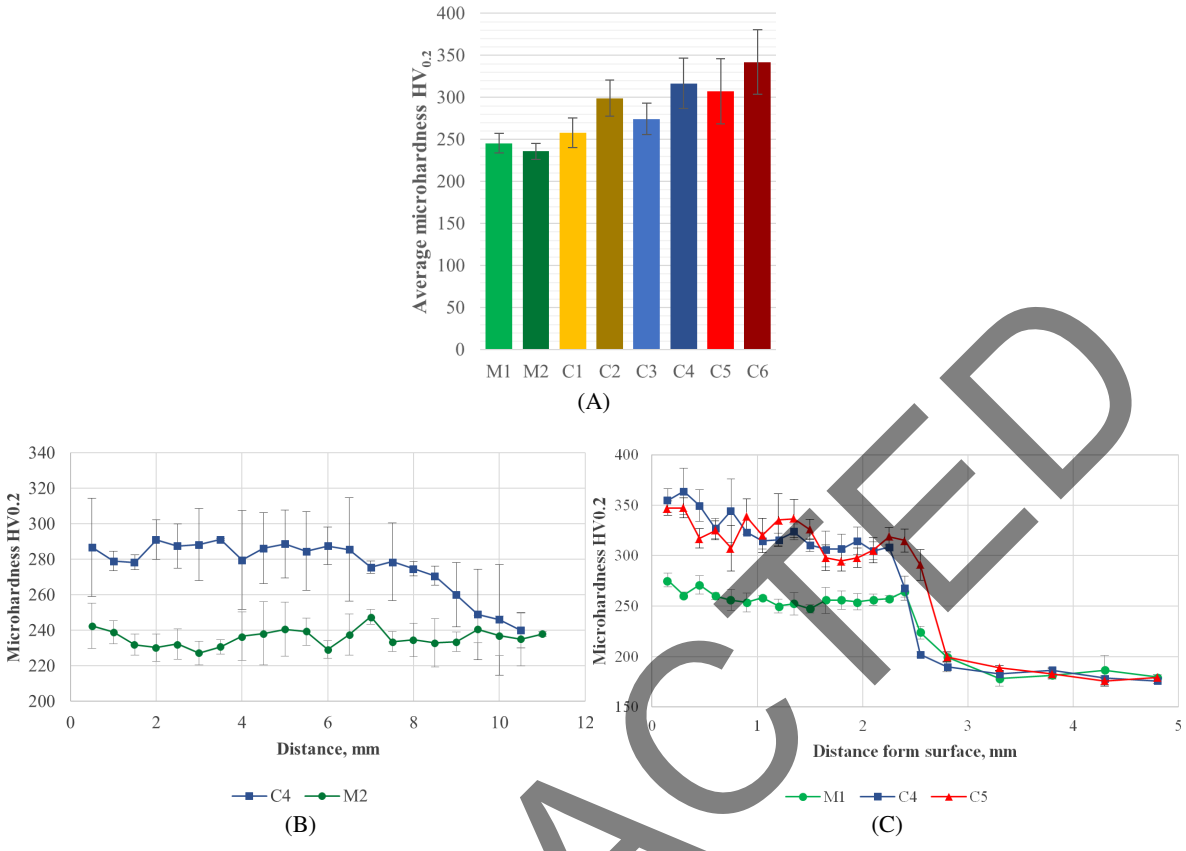

Fig. 10. Vickers microhardness results: **(A)** average microhardness, **(B)** microhardness distribution across the beads, and **(C)** microhardness distribution from the surface to the base material (designation according to Table 3)

RETRACTED

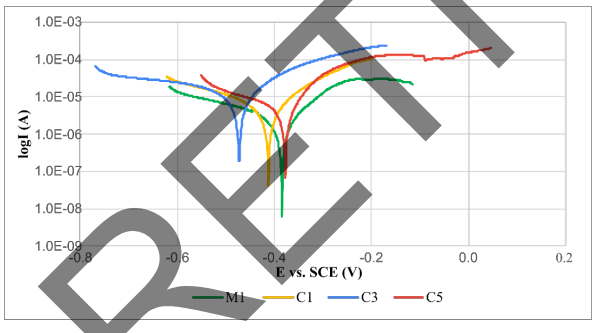

Fig. 11. Potentiodynamic polarization curves of M1, C1, C3, and C5 laser cladded coatings (designation according to Table 3). SCE, saturated calomel electrode

of the tested composite coatings, the C5 coating showed the highest corrosion resistance (similar to the metallic Inconel 625 coating) due to the highest structure homogeneity.

Table 5. Electrochemical parameters of laser-cladded coatings (designation according to Table 2)

Designation	j_{corr} **(μA/cm^2)**	E_{corr} **(V)**
M1	8.0	−0.384
C1	12.0	−0.412
C3	83.0	−0.473
C5	8.9	−0.377

The morphologies of corrosion damage of tested metallic and composite coatings are presented in Figure 12. The observations of surface morphology after the corrosion tests revealed the corrosion pits on the metallic and composite coatings. In the case of C1 and C3 coatings additionally, the passive film peeling was observed, which is evidence of the insufficient corrosion resistance in the NaCl solution (stability of the passive film determines the corrosion resistance of materials). The

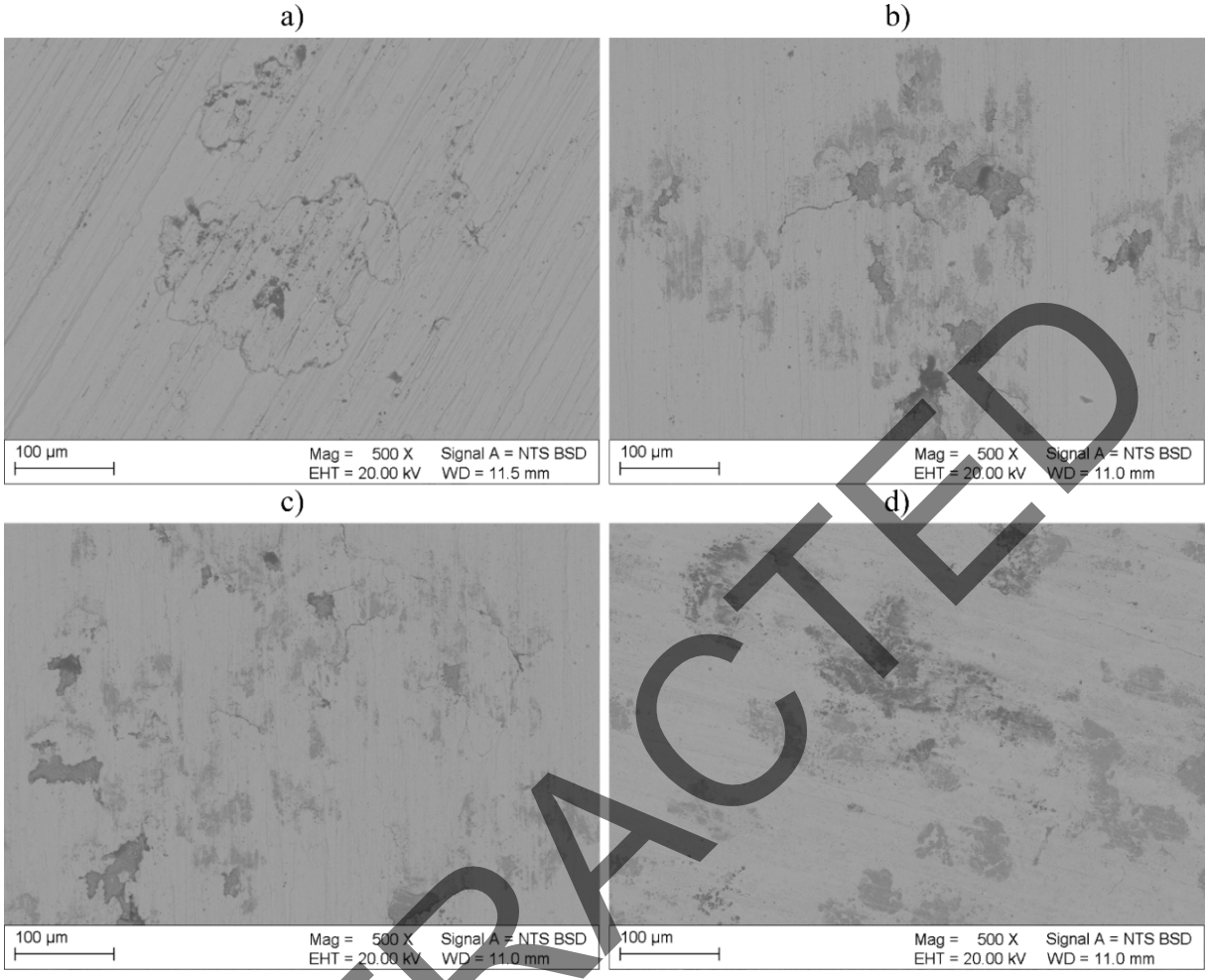

Fig. 12. Morphologies of corrosion damage after potentiodynamic polarization tests, SEM, and coatings: **(A)** M1, **(B)** C1, **(C)** C3, and **(D)** C5. SEM, scanning electron microscope; EHT, electron high tension voltage; BSD, backscattered electron detector; WD, working distance

RETRACTED

observations confirmed that in the case of C5 coating, the damage was the lowest out of the composite coatings (no passive film peeling was observed), but out of all tested coatings, Inconel 625 showed the lowest corrosion damage of the surface.

Thus, the results showed that the metallic Inconel 625 coatings are characterized by better corrosion resistance than the composite coatings reinforced with TiC particles, but by ensuring the high homogeneity of the composite coating structure, it is possible to receive similar corrosion resistance to Inconel 625.

4. Conclusions

The research on the production of the Inconel 625-based composite coatings reinforced with TiC particles allowed the following conclusions to be drawn:

1. The laser cladding process may be used for the production of homogeneous Inconel 625-based ex situ composite coatings reinforced with up to 40 vol.% of TiC particles. The powder feed rate parameter with constant laser beam power and speed has an influence on penetration and dilution of coat-

ings and no significant influence on homogeneity.

2. The TiC particles during the laser cladding process partially dissolved in the liquid pool, which resulted in the enrichment of the matrix in carbon and titanium. During the crystallization, the minor blocky secondary phases rich in carbon, titanium, niobium, and molybdenum precipitated. The TiC particle dissolution was more intense in the overlap area and resulted in the additional formation of dendritic precipitates rich in carbon, titanium, niobium, and molybdenum.
3. The average microhardness of composite Inconel 625/TiC coatings is higher than that of metallic Inconel 625 coatings and varies from 258 to 342 HV0.2. Together with the increase in the TiC fraction, the average microhardness of coatings increased. The coating dilution increase with the decrease in the powder feed rate resulted in the decrease in average microhardness. In the overlap areas, no significant or repeated microhardness changes were noted.
4. The Inconel 625 coating presents high corrosion resistance in a 3.5% NaCl solution. The corrosion resistance of composite TiC-reinforced coatings is lower than that of metallic coating.

References

[1] Mehta J, Mittal VK, Gupta P. Role of thermal spray coatings on wear, erosion and corrosion behavior: a review. J Appl Sci Eng. 2017;20(4):445–452. https://doi.org/10.6180/jase.2017.20.4.05

[2] Lisiecki A. Tribology and surface engineering. Coatings. 2019;9(10):663. https://doi.org/10.3390/coatings9100663

[3] Ostovan F, Hasanzadeh E, Toozandehjani M, Shafiei E, Jamaluddin KR, Amrin A. Microstructure, hardness and corrosion behavior of gas tungsten arc welding clad inconel 625 super alloy over A517 carbon steel using ERNiCrMo3 filler metal. J Mater Eng Perform. 2020;29:6919–6930. https://doi.org/10.1007/s11665-020-05178-x

[4] Jamrozik W, Górka J, Wyględacz B, Kiel-Jamrozik M. FEM-based thermogram correction for Inconel 625 joint hardness clustering. Materials. 2022;15(3):1113. https://doi.org/10.3390/ma15031113

[5] Scendo M, Staszewska-Samson K, Danielewski H. Corrosion behavior of Inconel 625 coating produced by laser cladding. Coatings. 2021;11(7):759. https://doi.org/10.3390/coatings11070759

[6] Czupryński A, Żuk M. Matrix composite coatings deposited on AISI 4715 steel by powder plasma-transferred arc welding. Materials. 2021;14(20):6066. https://doi.org/10.3390/ma14206066

[7] Lont A, Górka J, Janicki D, Matus K. The laser alloying process of ductile cast iron surface with titanium powder in nitrogen atmosphere. Coatings. 2022;12(2):227. https://doi.org/10.3390/coatings12020227

[8] Abioye TE, McCartney DG, Clare AT. Laser cladding of Inconel 625 wire for corrosion protection. J Mater Process Technol. 2015;217:232–40. https://doi.org/10.1016/j.jmatprotec.2014.10.024

[9] Janicki D, Musztyfaga-Staszuk M. Direct diode laser cladding of Inconel 625/WC composite coatings. J Mech Eng. 2016;62:363–72. https://doi.org/10.5545/sv-jme.2015.3194

[10] Janicki D. Laser cladding of Inconel 625-based composite coatings reinforced by porous chromium carbide particles. Opt Laser Technol. 2017;94:6–14. https://doi.org/10.1016/j.optlastec.2017.03.007

[11] Nurminen J, Nakki J, Vuoristo P. Microstructure and properties of hard and wear resistant MMC coatings deposited by laser cladding. Int J Refract Met Hard Mater. 2009;27:472–8. https://doi.org/10.1016/j.ijrmhm.2008.10.008

[12] Xu X, Mi G, Xiong L, Jiang P, Shao X, Wang C. Morphologies, microstructures and properties of TiC particle reinforced Inconel 625 coatings obtained by laser cladding with wire. J Alloys Compd. 2018;740:16–27. https://doi.org/10.1016/j.jallcom.2017.12.298

[13] Kim SH, Shin GH, Kim BK, Kim KT, Yang DY, Aranas C, et al. Thermo-mechanical improvement of Inconel 718 using ex situ boron nitride-reinforced composites processed by laser powder bed fusion. Sci Rep. 2017;7:14359. https://doi.org/10.1038/s41598-017-14713-1

[14] Shivalingaiah K, Sridhar KS, Sethuram D, Shivananda Murhty KV, Koppad PG, Ramesh CS. HVOF sprayed Inconel 718/cubic boron nitride composite coatings: microstructure, microhardness and slurry erosive behaviour. Mater Res Express. 2019;6(12):1265i8. Available from: https://iopscience.iop.org/article/10.1088/2053-1591/ab7067/meta

[15] Tang B, Tan Y, Zhang Z, Xu T, Sun Z, Li X. Effects of process parameters on geometrical characteristics, microstructure and tribological properties of TiB2 reinforced Inconel 718 alloy composite coatings by laser cladding. Coatings. 2020;10:76. https://doi.org/10.3390/coatings10010076

[16] Zhou S, Xu T, Hu C, Wu H, Liu H, Ma X. A comparative study of tungsten carbide and carbon nanotubes reinforced Inconel 625 composite coat-

RETRACTED

ings fabricated by laser cladding. Opt Laser Technol. 2021;140:106967. https://doi.org/10.1016/j.optlastec.2021.106967

[17] Deng P, Yao C, Feng K, Huang X, Li Z, Li Y, et al. Enhanced wear resistance of laser cladded graphene nanoplatelets reinforced Inconel 625 superalloy composite coating. Surf Coat Technol. 2018;335:334–44. https://doi.org/10.1016/j.surfcoat.2017.12.047

[18] Kotarska A, Poloczek T, Janicki D. Characterization of the structure, mechanical properties and erosive resistance of the laser cladded Inconel 625-based coatings reinforced by TiC particles. Materials. 2021;14:2225. https://doi.org/10.3390/ma14092225

[19] Galevsky GV, Rudneva VV, Garbuzova AK, Valuev DV. Titanium carbide: nanotechnology, properties, application. IOP Conf Ser Mater Sci Eng. 2015;91:012017. https://doi.org/10.1088/1757-899X/91/1/012017

[20] Gopinath M, Mullick S, Nath AK. Development of process maps based on molten pool thermal history during laser cladding of Inconel 718/TiC metal matrix composite coatings. Surf Coat Technol. 2020;399:126100. https://doi.org/10.1016/j.surfcoat.2020.126100

[21] Cao S, Gu D. Laser metal deposition additive manufacturing of TiC/Inconel 625 nanocomposites: relation of densification, microstructures and performance. J Mater Res. 2015;30(23):3616–28. https://doi.org/10.1557/jmr.2015.358

[22] Jiang D, Hong C, Zhong M, Alkhayat M, Weisheit A, Gasser A, et al. Fabrication of nano-TiCp reinforced Inconel 625 composite coatings by partial dissolution of micro-TiCp through laser cladding energy input control. Surf Coat Technol. 2014;249:125–31. https://doi.org/10.1016/j.surfcoat.2014.03.057

[23] Lian G, Zhang H, Zhang Y, Yao M, Huang X, Chen C. Computational and experimental investigation of microhardness and wear resistance of Ni-based alloy and TiC composite coating obtained by laser cladding. Materials. 2019;12(5):793. https://doi.org/10.3390/ma12050793

[24] Ge T, Chen L, Gu P, Ren X, Chen X. Microstructure and corrosion resistance of TiC/Inconel 625 composite coatings by extreme high speed laser cladding. Opt Laser Technol. 2022;150:107919. https://doi.org/10.1016/j.optastec.2022.107919

[25] Bakkar A, Ahmed MMZ, Alsaleh NA, El-Sayed Seleman MM, Ataya S. Microstructure, wear, and corrosion characterization of high TiC content Inconel 625 matrix composites. J Mater Res Technol. 2019;8(1):1102–1110. https://doi.org/10.1016/j.jmrt.2018.09.001

[26] Poloczek T, Janicki D, Górka J, Kotarska A. Effect of Ti and C alloyants on the microstructure of laser cladded cobalt-chromium coatings. IOP Conf Ser Mater Sci Eng. 2021;1182:012063. https://doi.org/10.1088/1757-899X/1182/1/012063

[27] Janicki D. Shaping the structure and properties of surface layers of ductile cast iron by laser alloying. Gliwice, Poland: Wydawnictwo Politechniki Śląskiej; 2018. p. 50.

[28] Cieslak MJ, Headley TJ, Romig AD, Kollie T. A melting and solidification study of alloy 625. Metall Mater Trans A 1988;19A:2319–31. Available from: doi:10.1007/BF02645056

[29] Kotarska A. The laser alloying process of ductile cast iron surface with titanium. Metals. 2021;11(2):282. Available from doi: 10.3390/met11020282

[30] Łyczkowska K, Michalska J. Studies on the corrosion resistance of laser-welded Inconel 600 and Inconel 625 nickel-based superalloys. Arch Metall Mater 2017;62(2):653–6. https://doi.org/10.1515/amm-2017-0100

[31] Shvets VA, Lavrenko VA, Talash VN, Panasyuk AD, Rudenko YB. Anodic polarization of titanium carbide TiCx in 3% NaCl solution in the homogeneity range. Powder Metall Met Ceram. 2016;55:113–23. https://doi.org/10.1007/s11106-016-9829-5

Received 2022-07-12
Accepted 2022-08-16

RETRACTED